JOURNAL OF SOLID STATE CHEMISTRY 54, 100–107 (1984)

Tracer Diffusion Coefficient of Oxide Ions in $LaCoO_3$ Single Crystal

TAKAMASA ISHIGAKI, SHIGERU YAMAUCHI, JUNICHIRO MIZUSAKI, AND KAZUO FUEKI

Department of Industrial Chemistry, University of Tokyo, Hongo, Bunkyo-ku, Tokyo 113, Japan

AND HIFUMI TAMURA

Central Research Laboratory, Hitachi Limited, Higashi-koigakubo, Kokubunji, Tokyo 185, Japan

Received October 28, 1983; in revised form February 15, 1984

The tracer diffusion coefficient, D_δ^*, of oxide ions in $LaCoO_3$ single crystal was determined over the temperature range of 700–1000°C by a gas–solid isotopic exchange technique using ^{18}O tracer. For the determination, two methods, the gas phase analysis and the depth profile measurement, were employed. Under an oxygen pressure of 34 Torr, the temperature dependence of D_δ^* in $LaCoO_3$ was expressed by

$$D_\delta^*(\mathrm{cm^2 \cdot sec^{-1}}) = 3.63 \times 10^4 \exp\left\{-\frac{(74 \pm 5)\mathrm{kcal \cdot mole^{-1}}}{RT}\right\}.$$

D_δ^* at 950°C was found to be proportional to $P_{O_2}^{-0.35}$. The diffusion of oxide ions occurs through a vacancy mechanism. The activation energy for the migration of oxide ion vacancies was estimated as 18 kcal · $mole^{-1}$.

1. Introduction

Recently, applications of perovskite-type oxides have been extensively developed and the properties of these oxides have been intensively investigated. It is thought that many perovskite-type oxides have high oxide ion diffusivity (*1–3*). However, few measurements have been reported on the tracer diffusion coefficient of oxide ions in perovskite-type oxides. They are limited to titanates: $SrTiO_3$ (*4–6*), $BaTiO_3$ (*7*), and impurity-doped $SrTiO_3$ (*5*) and $BaTiO_3$ (*7*). It has been suggested that the diffusion of oxide ions proceeds via oxide ion vacancies, but this diffusion mechanism has not been experimentally confirmed.

The perovskite-type oxides, $Ln_{1-x}Sr_xCoO_3$ (*Ln:* rare earth elements), have been investigated for applications as oxidation catalysts (*8, 9*), electrode materials of fuel cells (*10–12*), and chemical sensors (*13*). Substitution of a part of Ln^{3+} in $LaCoO_3$ by Sr^{2+} increases Co^{4+} and oxide ion vacancies. The increase of Co^{4+} leads to the high electronic conductivity, which has been considered to be important in applications. In addition, high oxide ion diffusivity resulting from a large concentration of vacancies in indispensable for the high reactivity observed in applications (*9, 11, 12*). However, few diffusion data were reported. Only a chemical diffusion coefficient has been determined at lower temperatures on

0022-4596/84 $3.00

polycrystalline samples of $Nd_{1-x}Sr_xCoO_3$(x = 0.2, 0.5) (*11*) and $La_{0.5}Sr_{0.5}CoO_3$ (*12*) by means of electrochemical methods. Therefore the diffusion coefficients of oxide ions in these materials are needed for further development of applications of these materials. $LaCoO_3$ has been chosen as a model compound in this work, because $La_{1-x}Sr_xCoO_3$ is the most popular among these compounds. It has been reported that $La_{1-x}Sr_xCoO_{3-\delta}$ is characterized by a large oxygen deficiency, depending on temperature and oxygen pressure (*12, 14, 15*). Accordingly, care has to be taken to control the nonstoichiometric composition in the diffusion experiments.

Oxygen has no radioactive isotope suitable for use as a tracer in diffusion experiments. Most previous studies on tracer diffusion of oxide ions in oxides, therefore, have used the gas–solid isotopic exchange technique in which the amount of isotope taken up by a sample is determined by monitoring the isotopic composition in the atmosphere. The analysis of exchange data is quite complicated if the surface exchange rate is low (*16*). Recent advances in performance of secondary ion mass spectrometers, SIMS, have made it possible to determine the depth profile of isotopes with high accuracy, and the SIMS technique has begun to be used for the measurements of tracer diffusion coefficient (*17–21*). SIMS has the advantage of directly determining concentration profiles in solids. In the present paper, both methods, that is, the gas phase analysis and the depth profile measurement by means of SIMS, have been employed.

2. Experimental Procedure

2.1 Materials

$LaCoO_3$ powder was prepared by a coprecitipation method. Using this powder, rods of single crystal of 4 mm in diameter and 40 mm in length were grown by the floating zone method utilizing a xenon arc image furnace (*22*); the details are described elsewhere (*23*).

After single crystals were annealed at 1200°C in air for 2 days, they were cut into blocks or slabs by a wire blade. Spheres of 3–4 mm in diameter were fabricated from blocks using emery paper. They were used for the experiments of the gas phase analysis. For the depth profile measurement, slabs of 0.7–0.8 mm thickness were finely polished using 0.05-μm alumina polishing powder.

2.2 Diffusion Annealings and Measurements

(*a*) *Diffusion annealings.* An infrared image furnace, Shinku-Riko RH-L, was employed for the diffusion anneal. In the furnace four halogen lamps were employed as heating element, and infrared light was focused by four concave mirrors at the center of the reactor. This furnace enabled us to heat up and quench a sample rapidly.

The reactor is made of a silica-glass tube. A Pt–Pt13Rh thermocouple was set at the center of the reactor. A platinum crucible was hung right under the thermocouple. The sample was contained in the platinum crucible to avoid the direct irradiation by the halogen lamps. By a blank test it was confirmed that no isotopic exchange reaction occurred between the wall of reactor and the oxygen gas

Diffusion annealings were made in 21.5% ^{18}O-enriched oxygen gas (Prochem., Cat. No. 00-409, B.O.C. Limited, U.K.), after the sample had been annealed at the desired temperature and oxygen pressure for 10–18 hr. The preannealing was carried out in order to equilibrate the defect concentration with the same oxygen atmosphere of diffusion annealing, and to remove mechanical damage on the surface of the sample.

(*b*) *Gas phase analysis.* The decrease in $^{18}O/^{16}O$ ratio in the gas phase was followed

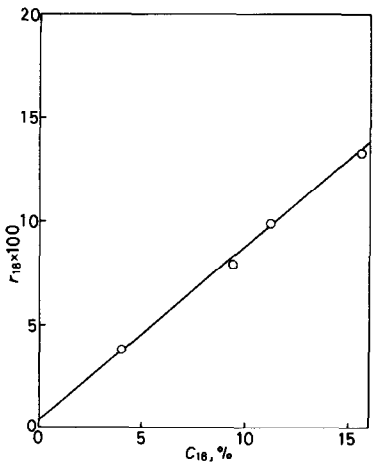

FIG. 1. Calibration curve for the ^{18}O concentration by means of SIMS.

by a quadrupole mass spectrometer, Nichiden Anelva NAG-531. For the conversion of peak intensities to $^{18}O/^{16}O$ ratios, a calibration was carried out before and after each diffusion annealing, using 21.5% ^{18}O-enriched oxygen gas.

(*c*) *Depth profile measurement.* A slab sample was annealed in ^{18}O-enriched gas for a predetermined time, and the depth profile of the oxygen isotopic composition was obtained by measuring the intensities of negative singly charged ions by means of a Hitachi ion microanalyzer, IMA-II (*24*). Operating parameters during analysis were as follows: the primay ions are Ar^+, primary ion energy 13 keV, spot size on the sample surface 100 μm, and rastered area of beams 300 × 300 μm. The Ar^+ beam was rastered to etch the sample surface and stopped at the center of the rastered area to measure the isotopic composition. Then this procedure was repeated. The depth of the ion-etched crater was measured by a Talystep profilometer after measurement.

In the SMS measurement on oxygen isotopic composition, the intensity ratios of isotopic peaks are influenced by the gaseous oxygen in a SIMS chamber and the primary ion current density (*25*). As a result, the value of mass peak intensity ratio, $r_{18} = I_{18}/(I_{16} + I_{18})$ becomes small compared to the ^{18}O concentration in solid, C_{18}, when the primary ion current density is low. Therefore, the following calibration was carried out in order to determine the relation between r_{18} and C_{18}: The slab samples with uniform ^{18}O concentration of 4.0, 9.4, 11.2, and 15.6% were prepared by annealing them for 170 hr, which was sufficient for the complete isotopic exchange. A calibration curve was formed by plotting r_{18} against C_{18}. Utilizing the calibration curve, the intensity ratio, r_{18}, was converted into the concentration, C_{18}. Typical results are given in Fig. 1. Calibration curves were carried out at every depth profile measurement.

3. Results and Discussion

3.1 Gas Phase Analysis

The diffused amounts, M_t/M_∞, of ^{18}O against time were determined by the ratio of isotopic composition of ^{16}O and ^{18}O in the gas phase, as shown in Fig. 2, where M_t and M_∞ represent the total ^{18}O amounts diffusing in the solid for a time t and infinite time, respectively.

When the isotopic exchange process is rate-controlled by bulk diffusion, the solu-

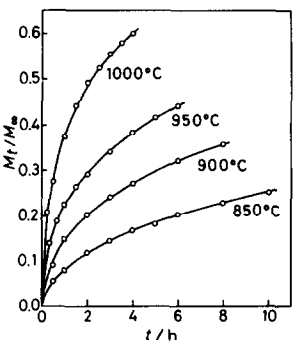

FIG. 2. Diffused amounts of oxygen against time in the gas phase analysis: P_{O_2} = 34 Torr.

tion of diffusion equation with the present boundary condition is given by (*26*)

$$\frac{M_t}{M_\infty} = 1 - \sum_{n=1}^{\infty} \frac{6\alpha(1+\alpha)}{9 + 9\alpha + \alpha^2 q_n^2} \exp\left(-\frac{Dq_n^2 t}{a^2}\right) \quad (1)$$

$$\tan q_n = \frac{3q_n}{3 + \alpha q_n^2} \quad (2)$$

where D is the diffusion coefficient, α the atomic ratio of oxygen in the gas phase and the solid phase, a the radius of the sphere sample, q_n the nonzero positive root of Eq. (2).

Dt, corresponding to M_t/M_∞ were calculated by using Eq. (1), and plotted against t in Fig. 3. Under the condition in which Eq. (1) is satisfied, the plots should show a straight line. However, slightly concave curves were obtained, as shown in the figure. This indicates that the present isotopic exchange was partially controlled by the surface exchange reaction.

Accordingly, the observed data were fitted to Eq. (3) in which the rate of surface reaction was taken into account (*27*);

$$\frac{M_t}{M_\infty} = 1 - \sum_{n=1}^{\infty} \frac{6\alpha M^2(1+\alpha)}{\alpha^2 q_n^4 + \alpha M\{\alpha(M-1) - 6\}q_n^2 + 9(1+\alpha)M^2} \exp\left(-\frac{Dq_n^2 t}{a^2}\right) \quad (3)$$

$$\tan q_n = \frac{3Mq_n - \alpha q_n^3}{\alpha q_n^2(M-1) + 3M}, \qquad M = ka/D \quad (4)$$

where k is the rate constant of the surface exchange reaction, and q_n, the nonzero roots of Eq. (4).

D and k were determined by a least-square analysis using SALS program package at the Computer Center of the University of Tokyo. The results are given in Table I. The solid lines in Fig. 2 are those calculated using the determined D and k. They agree well with the observed values.

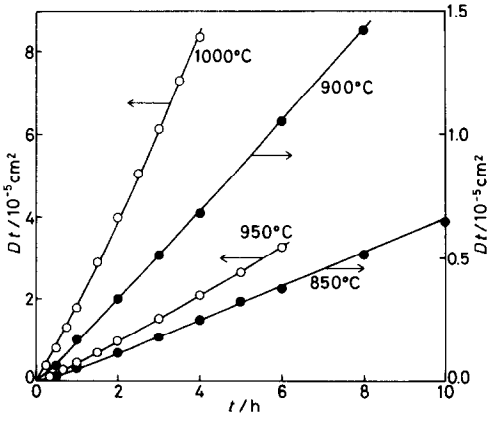

FIG. 3. Plots of Dt gainst t for the gas phase analysis.

3.2 Depth Profile Measurement

The ^{18}O concentration profiles in the solid phase as determined by SIMS are shown in Fig. 4.

The one-dimensional solution of the diffusion equation in a semiinfinite medium

TABLE I

TRACER DIFFUSION COEFFICIENT, D_O^*, OF OXIDE IONS AND DIFFUSION COEFFICIENT, D_V, OF OXIDE ION VACANCIES DETERMINED BY THE GAS PHASE ANALYSIS

t (°C)	P_{O_2} (Torr)	D_O^* ($cm^2 \cdot sec^{-1}$)	k ($cm \cdot sec^{-1}$)	log δ^a	D_V ($cm^2 \cdot sec^{-1}$)
1000	34	6.29×10^{-9}	9.35×10^{-6}	−2.90	1.36×10^{-5}
		5.15×10^{-9}	1.91×10^{-5}		
950	80	1.19×10^{-9}	4.48×10^{-6}	−3.43	9.61×10^{-6}
	49	1.35×10^{-9}	5.34×10^{-5}	−3.33	8.66×10^{-6}
	34	1.74×10^{-9}	2.76×10^{-6}	−3.26	8.52×10^{-6}
		1.27×10^{-9}	4.39×10^{-5}		
	16	2.04×10^{-9}	2.26×10^{-6}	−3.10	7.70×10^{-6}
900	34	5.28×10^{-10}	3.17×10^{-6}	−3.61	6.81×10^{-6}
		5.85×10^{-10}	8.64×10^{-5}		
850	34	2.12×10^{-10}	9.15×10^{-7}	−3.98	5.13×10^{-6}
		1.45×10^{-10}	1.29×10^{-6}		

[a] Determined by thermogravimetry (*31*).

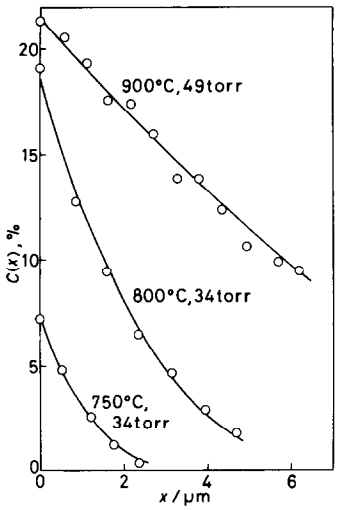

FIG. 4. Concentration profiles of ^{18}O obtained by SIMS.

with a boundary of constant atmospheric concentration is given by (*28*),

$$\frac{C(x)}{C_g} = \operatorname{erfc}\left(\frac{x}{2\sqrt{Dt}}\right) - \exp(hx + h^2Dt) \operatorname{erfc}\left(\frac{x}{2\sqrt{Dt}} + h\sqrt{Dt}\right) \qquad h = k/D \quad (5)$$

where $C(x)$ and C_g are the ^{18}O concentrations at a distance x from the surface and in the gas phase, respectively. D and k were determined by fitting data to Eq. (5) in the same way as for the gas phase analysis. The results are presented in Table II.

3.3 Dependence of Tracer Diffusion Coefficient on Temperature and Oxygen Pressure

In the measurements of depth profile using SIMS, the diffusion length should be limited to less than 10 μm, because of the need for stability of the primary ion current for a long time and the uncertainty arising from the secondary ion current emitted at the bottom of the crater. As a result, there is an upper limit in $D_O^* t$ which can be determined by the depth profile measurement. It is considered that the shortest annealing time with satisfactory accuracy is 10 min. This penetration depth and annealing time limit the largest value of D_O^* to 5×10^{-10} cm^2 · sec^{-1}. Where D_O^* is more than 5×10^{-10} cm^2 · sec^{-1}, the gas phase analysis should be carried out. At a temperature of 900°C and a pressure of 34 Torr, tracer diffusion coefficients were obtained by both the gas phase analysis and the depth profile measurement. Tables I and II show that both values agree with each other within experimental error. As discussed in the following section, the diffusion coefficient, D_V, of oxide ion vacancies, which is calculated from D_O^*, is independent of oxygen

TABLE II

TRACER DIFFUSION COEFFICIENT, D_O^*, OF OXIDE IONS AND DIFFUSION COEFFICIENT, D_V, OF OXIDE ION VACANCIES DETERMINED BY THE DEPTH PROFILE MEASUREMENT

t (°C)	P_{O_2} (Torr)	Annealing time (min)	D_O^* (cm^2 · sec^{-1})	k (cm · sec^{-1})	log δ[a]	D_V (cm^2 · sec^{-1})
900	49	10	5.31×10^{-10}	—[b]	−3.68	7.70×10^{-6}
			5.41×10^{-10}	—[b]		
	34	10	5.96×10^{-10}	1.41×10^{-6}	−3.61	7.28×10^{-6}
850	49	15	1.52×10^{-10}	—[b]	−4.05	5.12×10^{-6}
800	34	30	2.41×10^{-11}	3.47×10^{-7}		
750	34	60	3.42×10^{-12}	1.30×10^{-8}		
700	34	150	9.20×10^{-13}	4.57×10^{-9}		

[a] Determined by thermogravimetry (*31*).
[b] Iteration did not converge in the calculation.

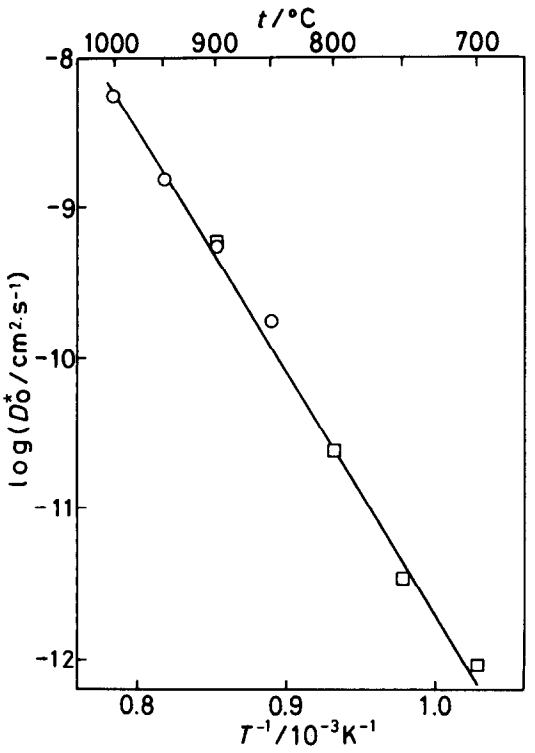

FIG. 5. Arrhenius plots of tracer diffusion coefficient of oxide ions in $LaCoO_3$ single crystal. ○; Determined by the gas phase analysis. □; Determined by the depth profile measurement.

pressure. At both temperatures of 900 and 850°C, D_V obtained by both methods were in good agreement. So far the tracer diffusion coefficient obtained using SIMS technique have been determined independently of other methods. Comparisons of both results have been made for measurements by different workers on different sample specimens. In the present investigation a comparison was carried out on the same sample specimens. It is confirmed that the results by both methods agreed quite well. It is concluded that the depth profile measurement is as relevant as the gas phase analysis to the determination of diffusion coefficients.

The Arrhenius plot of tracer diffusion coefficient at an oxygen pressure of 34 Torr is shown in Fig. 5. The temperature dependence is expressed by the equation

$$D_O^*/\mathrm{cm}^2 \cdot \mathrm{sec}^{-1} = 3.63 \times 10^4 \exp\left(-\frac{(74 \pm 5)\mathrm{kcal} \cdot \mathrm{mole}^{-1}}{RT}\right) \quad (6)$$

(where the digit following ± denotes 2σ).

Figure 6 shows the dependence of tracer diffusion coefficient on oxygen pressure at 950°C. The data were obtained by the gas phase analysis. It is shown that D_O^* decreases with an increase in oxygen pressure, and that D_O^* is proportional to $P_{O_2}^{-(0.35\pm0.04)}$. It is well established that when diffusion proceeds via point defects and if the defects are randomly distributed, the self-diffusion coefficient should be proportional to the concentration of point defects (*29, 30*),

$$D_i = N_d D_d \quad (7)$$

where D_i is the self-diffusion coefficient of species i, N_d is the mole fraction of point defects in the crystal, and D_d is the diffusion coefficient of point defects. The concentration of oxide ion vacancies decreases with an increase in oxygen pressure. The present dependence of D_O^* on oxygen pressure suggests that point defects which are

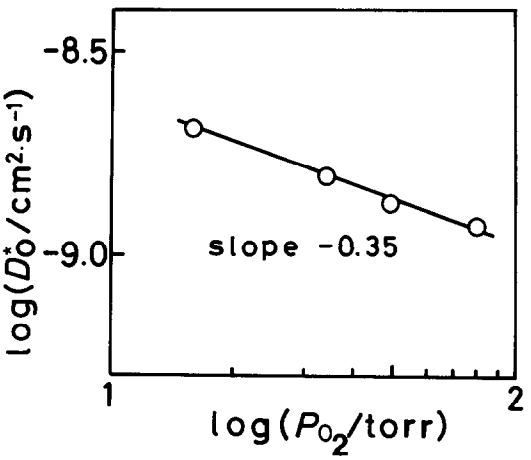

FIG. 6. Dependence of tracer diffusion coefficient of oxide ions of $LaCoO_3$ on oxygen pressure at 950°C.

responsible for diffusion are oxide ion vacancies.

Seppänen and his coinvestigators measured the nonstoichiometry in oxygen-deficient $LaCoO_{3-\delta}$ at 1170–1131 K by coulometric titration, using a solid electrolyte emf cell (*15*). They have reported that the nonstoichiometry δ is proportional to $P_{O_2}^{-0.5}$ and concluded that oxide ion vacancies are majority defects in oxygen-deficient $LaCoO_{3-\delta}$. Their result indicate that the concentration of oxide ion vacancies is proportional to $P_{O_2}^{-0.5}$. Also, the nonstoichiometric isotherms were explained by a model in which oxide ion vacancies are randomly distributed and the interaction between them is very weak. Mima and his coinvestigators have carried out the thermogravimetric study using a specimen cut from the same crystal as used in the present work, to determine the nonstoichiometry as a function of oxygen partial pressure (*31*). They obtained the same result as Seppänen and his coinvestigators that the nonstoichiometry δ was proportional to $P_{O_2}^{-0.5}$. Considering the experimental error in the tracer diffusion coefficient and the experimental limitation of variable oxygen pressure range and using Eq. (7), it is concluded that the present result of $D_O^* \propto P_{O_2}^{-(0.35\pm0.04)}$ agrees with the two prior results on oxygen partial pressure dependence of nonstoichiometry.

3.4 Diffusion Coefficient of Oxide Ion Vacancies

Based on the defect model mentioned in the preceding section (*15, 31*), the diffusion coefficient, D_V, of oxide ion vacancies can be calculated from the tracer diffusion coefficient. For the perovskite-type $ABO_{3-\delta}$, Eq. (7) is rewritten as

$$D_O^* = N_V D_V = \frac{\delta}{3} D_V \qquad (8)$$

where the correlation factor is assumed to be unity and N_V is the mole fraction of oxide ion vacancies in the oxide ion lattice sites. For the calculation of D_V, δ shown in

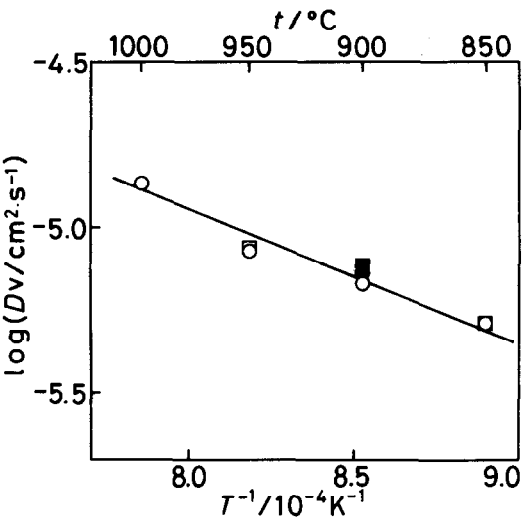

FIG. 7. Diffusion coefficient of oxide ion vacancies in $LaCoO_3$. ○,●; P_{O_2} =34 Torr. □,■; P_{O_2} = 49 Torr. ○,□; Determined by the gas phase analysis. ●,■; Determined by the depth profile measurement.

Tables I and II, which was determined by the thermogravimetry (*31*), was used. The calculated D_V are given in Tables I and II, and Fig. (7). The errors inherent in D_O^* and δ are of about 10–20%, and the error in D_V is of several tens of a percent.

In Fig. 7, it is seen that the Arrhenius plots of D_V determined from the D_O^* by the different two methods and at the different oxygen pressure fall on the same line. The temperature dependence is expressed by the equation

$$D_V(\text{cm}^2 \cdot \text{sec}^{-1}) = 1.59 \times 10^{-2} \exp\left(-\frac{(18 \pm 5)\text{kcal} \cdot \text{mole}^{-1}}{RT}\right). \qquad (9)$$

The activation energy of D_V, 18 kcal · mole^{-1}, corresponds to the migration energy, ΔH_m, of oxide ion vacancies in $LaCoO_3$.

The activation energy for the tracer diffusion coefficient is a sum of the formation energy, ΔH_f, and the migration energy, ΔH_m of point defects (*32*). The formaion energy of oxide ion vacancies may be calculated by the relation

$$\left(\frac{\partial \ln \delta}{\partial(1/T)}\right)_{P_{O_2}} = -\frac{\Delta H_f}{R}. \qquad (10)$$

The values of ΔH_f obtained from the nonstoichiometric data by Seppänen and his coinvestigators (*15*) and Mima and his coinvestigators (*31*) are 52 and 50 kcal · mole^{-1}, respectively. The sum of ΔH_f and ΔH_m are 71 and 69 kcal · mole^{-1}. As expected, both values agree with the activation energy of D_δ^*, (74 ± 5) kcal · mole^{-1}, obtained in the present work.

Acknowledgments

This work was partially supported by a grant-in-aid for Scientific Research (5820800) from the Ministry of Education, Japan.

References

1. T. Takahashi and H. Iwahara, *Denki Kagaku* **35,** 433 (1967).
2. T. Takahashi, H. Iwahara, and T. Ichimura, *Denki Kagaku* **37,** 857 (1969).
3. T. Takahashi and H. Iwahara, *Energy Convers.* **11,** 105 (1971).
4. A. E. Paladino, L. G. Rubin and J. S. Waugh, *J. Phys. Chem. Solids* **26,** 391 (1965).
5. A. Yamaji, *Acta Crystallogr. Sect. A* **A28** Suppl. S167 (1972); *J. Amer. Ceram. Soc.* **58,** 152 (1975); *Denki Tsushin Kenkyusho Kenkyu Jitsuyoka Hokoku* **25,** 1197 (1976).
6. R. Haul, K. Kübner, and O. Kircher, *in* "Proceedings, 8th International Symposium on Reactivity of Solids, 1976" (J. Wood, O. Lindqvist, and C. Helgesson, Eds.), p. 101, Plenum, New York (1977).
7. S. Shirasaki, H. Yamamura, H. Haneda, K. Kakegawa, and J. Moori, *J. Chem. Phys.* **73,** 4640 (1980).
8. M. W. Chien, I. M. Peason, and K. Nobe, *Ind. Eng. Chem., Prod. Res. Dev.* **14,** 131 (1975).
9. K. Sakata, T. Nakamura, M. Misono, and Y. Yoneda, *Chem. Lett.* 273 (1979).
10. F. R. van Buren, G. H. J. Broers, and T. G. M. van den Belt, *Ber. Bunsenges. Phys. Chem.* **83,** 82 (1979).
11. T. Kudo, H. Obayashi, and T. Gejo, *J. Electroanal. Chem.* **122,** 159 (1975).
12. F. R. van Buren, G. H. J. Broers, A. J. Bouman, and C. Boesveld, *J. Electroanal. Chem.* **88,** 353 (1978). A. G. C. Kobussen, F. R. van Buren, and G. H. J. Broers, *J. Electrochem.* **91,** 211 (1978).
13. H. Obayashi, Y. Sakurai and T. Gejo, *J. Solid State Chem.* **17,** 299 (1976).
14. H. Obayashi, T. Kudo, and T. Gejo, *Jpn. J. Appl. Phys.* **13,** 1 (1974).
15. M. Seppänen, M. Kytö, and P. Toskinen, *Scand. J. Metall.* **9,** 3 (1980).
16. M. Nanba, Y. Oishi, and K. Ando, *J. Chem. Phys.* **75,** 913 (1981).
17. M. Arita, M. Hosoya, M. Kobayashi, and M. Someno, *J. Amer. Ceram. Soc.* **62,** 443 (1979).
18. S. Yamaguchi and M. Someno, *Trans. Jpn. Inst. Met.* **23,** 259 (1982).
19. D. J. Reed and B. J. Wuench, *J. Amer. Ceram. Soc.* **63,** 88 (1982).
20. J. A. Kilner, J. Drennan, P. Dennis, and B. C. H. Steele, *Solid State Ionics* **5,** 527 (1981).
21. R. Freer and P. F. Dennis, *Mineral. Mag.* **45,** 179 (1982).
22. K. Kitazawa, K. Nagashima, T. Mizutani, K. Fueki, and T. Mukaibo, *J. Cryst. Growth* **39,** 211 (1977).
23. T. Matsuura, T. Ishigaki, J. Mizusaki, S. Yamauchi, and K. Fueki, submitted for publication.
24. H. Tamura, T. Kondo, and T. Hirano, *in* "Proceedings, 6th International Conference on X-Ray Optics and Micro-Analysis, 1969" (G. Shinoda, K. Koda, and T. Ichinokawa, Eds.), p. 423, Univ. Tokyo Press, Tokyo (1971).
25. K. Sato, Y. Inoue, M. Ohno, H. Igarashi, and M. Someno, "Abstract of 4th International Conference on Secondary Ion Mass Spectrometry," p. 143 (1983).
26. J. Krank, "The Mathematics of Diffusion," 2nd ed., p. 94, Oxford Univ. Press, London/New York (1975).
27. H. S. Edwars, A. F. Rosenberg, and J. T. Bittel, Aeronautical Systems Division, Wright-Patterson Air Force, OH, Report ASD-TDR-63-635; July, 1963.
28. J. Crank, "The Mathematics of Diffusion," 2nd ed., p. 36, Oxford Univ. Press, London/New York (1975).
29. R. J. Friauf, *in* "Physics of Electrolyte" (J. Hladik, Ed.), Vol. 1, p. 153, Academic Press, New York/London (1972).
30. H. Schmalzried, "Solid State Reactions," Materials Science Series, p. 56, Verlag Chemie, Weinheim (1974).
31. Y. Mima, T. Ishigaki, J. Mizusaki, S. Yamauchi, and K. Fueki, "Proceedings, 10th Kotai Ionikusu Toronkai," p. 91, Mie, Japan (1983).
32. P. Kofstad, "Nonstoichiometry, Diffusion and Electrical Conductivity in Binary Metal Oxides," p. 80, Wiley, New York (1972).